Machine Learning and Modeling of Ultrasonic Signals for High-Fidelity Data Compression

Jafar Saniie[1], Pramod Govindan[1], Boyang Wang[1], Xin Zhang[1], Yufeng Lu[2], Erdal Oruklu[1]

Embedded Computing and Signal Processing Research Laboratory (http://ecasp.ece.iit.edu/)
[1]*Department of Electrical and Computer Engineering, Illinois Institute of Technology, Chicago, IL 60616*
[2]*Department of Electrical and Computer Engineering, Bradley University, Peoria, IL 61625*

***Abstract*— Ultrasonic systems are widely used in imaging applications for non-destructive evaluation, quality assurance, and medical diagnosis. These applications require large volumes of data to be processed, stored, and/or transmitted in real time. It is essential to compress the ultrasonic RF signal without inadvertently degrading desirable signal features. This study explores the development of learning models for massive data compression based on wavelet packet transformation, using machine learning techniques. Furthermore, this study utilizes the fast chirplet transform algorithm to successively estimate broadband, narrowband, symmetric, skewed, nondispersive, or dispersive echoes. These parameters not only have significant physical interpretations for radar, sonar, seismic, and ultrasonic applications but also, yield a method for efficient and high-precision data compression. Signal modeling and parameter estimation of the nonstationary ultrasonic echoes are critical for image analysis, target detection, and object recognition. The objective of this study is to design computationally efficient algorithms and the implementation of 3D ultrasonic data compression.**

I. Introduction

One of the major challenges in ultrasonic imaging applications is the large volumes of radio frequency (RF) data. The RF data compression helps to rapidly transmit the information to remote locations for archiving and further analysis. Raw RF signal preserves the important information within the signal [1] with direct and precise interpretation for applications such as medical diagnosis. In ultrasonic non-destructive evaluation applications, the backscattered RF signal possesses information about the geometric shape, size, and orientation of the scatterers within the propagation path [2, 3]. Finer details within the ultrasonic signal are extremely critical for tissue characterization, detection, and estimation of defects within materials. Therefore, compressed ultrasonic RF signal has to be strictly recoverable with very high signal accuracy. It is a common practice to oversample the signals for high-definition data to detect small and transient features within the signal. This helps to obtain a high time resolution so that the arrival time and the amplitude of the echoes can be precisely detected. However, this oversampling produces a large amount of data with redundant information, which needs to be eliminated during the compression.

In this paper, we introduce a chirplet signal decomposition (CSD) algorithm to represent chirp-type signals in terms of Gaussian chirplets, which are sparse and energy-preserving. The chirp signal is often encountered in ultrasound, sonar, radar, EEG, seismic signals, and speech [4]–[16]. The chirp signal parameters represent valuable information pertaining to the shape, size, and orientation of the reflectors in ultrasonic nondestructive evaluation, the location and velocity of the moving targets in radar-target detection, or the propagation path in seismic signal analysis. The decomposition allows a complex signal to be represented by a limited number of chirp components. Furthermore, due to the energy preservation property, a high-resolution TF representation is achieved by decomposing the signal into a limited number of chirp functions with known TF distributions [17]–[19]. Additionally, the nonstationary behavior of the signal can be described by the chirplet echoes. Based on the chirplet transform (CT) of the signal, the CSD method uses a successive parameter estimation algorithm to identify the location and duration of the most dominant chirp component in the TF domain and estimates the parameters of this dominant chirp component.

This paper also analyzes wavelet packet transform (WPT) [20,21] based on ultrasonic RF signal compression using sub-band elimination with maintaining a high compression ratio and high signal reconstruction quality. Carefully designed multistage sub-band decomposition structure along with the most suitable wavelet kernel helps to efficiently compress different kinds of signals based on the frequency localization. In this study, the compression performance of both the broadband and narrowband echoes are analyzed for multiple wavelet kernels. Volumetric information demands three-dimensional (3D) scanning and subsequently significant RF signal data collection. Thus, the compression of volumetric RF data becomes an essential part of the data analysis and diagnostic process. In this study, the compression is performed on a 3D block of data through successive 1D compression in each of the three directions (x, y and z). In particular, we analyze how the peak signal-to-noise ratio (PSNR) varies depending on the compression ratio (CR) and the correlation properties among 3D ultrasonic experimental measurements.

Furthermore, in this study, a wavelet packet transformation convolutional autoencoder (WPTCAE) is designed to improve the quality of ultrasonic signal compression. The autoencoder (AE) is an unsupervised learning model that can be used for signal compression, dimension reduction, feature extraction, and denoising [22]-[24]. The convolutional AE (CAE) comprises

convolution layers, which can achieve better performance with fewer trainable weights, especially when high-resolution images are processed [25]. This approach offers a considerable performance enhancement compared with WPT-based signal compression.

Section II describes ultrasonic signal modeling for signal analysis, noise reduction, and data compression. Section III explains the WPT compression. Section IV details the design of WPTCAE compression models.

II. Echo Model and Data Compression

In most detection applications, a single echo can be modeled as a chirplet [26], [27] as follows:

$$f_{\Theta}(t) = \beta \exp\left(-\alpha_1 (t-\tau)^2 + i2\pi f_c (t-\tau) + i\phi + i\alpha_2 (t-\tau)^2\right) \quad (1)$$

where

$$\Theta = [\tau, f_c, \alpha_1, \alpha_2, \phi, \beta\ ]$$

denotes the parameter vector. The term τ is the time-of-arrival, f_c is the center frequency, β is the amplitude, α_2 is the chirp rate, ϕ is the phase, and α_1 is the bandwidth factor of the echo. The chirplet transform of the echo is defined [26], [28] as follows:

$$CT\ (\hat{\Theta}) = \int_{-\infty}^{+\infty} f_{\Theta}(t) \Psi^{*}_{\hat{\Theta}}(t) dt \quad (2)$$

$$\Psi_{\hat{\Theta}}(t) = \eta \exp\left(-\gamma_1 (t-b)^2 + i\omega_0 \left(\frac{t-b}{a}\right) + i\theta + i\gamma_2 (t-b)^2\right) \quad (3)$$

denotes the chirplet kernel, and

$$\hat{\Theta} = \left[b, \frac{\omega_0}{2\pi a}, \gamma_1, \gamma_2, \theta, \eta\right]$$

$$\eta = \left(\frac{2\gamma_1}{\pi}\right)^{1/4}$$

denotes the parameter vector of the chirplet used for transformation, and the normalization factor. The parameter can be successively estimated [29] as shown in the following:

$$\left.\begin{aligned} \frac{\partial \left|\mathrm{CT}(\widehat{\Theta})\right|}{\partial a} = 0 \\ \frac{\partial \left|\mathrm{CT}(\widehat{\Theta})\right|}{\partial b} = 0 \end{aligned}\right\} \Rightarrow\ b = \tau\ \ and\ \ \frac{w_0}{a} = w_c \quad (4)$$

$$\left.\frac{\partial \mathrm{CT}(\widehat{\Theta})}{\partial \gamma_2}\right|_{b=\tau,\ \frac{w_0}{a}=w_c} = 0\ \Rightarrow\ \gamma_2 = \alpha_2 \quad (5)$$

$$\left.\frac{\partial \mathrm{CT}(\widehat{\Theta})}{\partial \gamma_1}\right|_{\substack{b=\tau, \\ \frac{w_0}{a}=w_c, \\ \gamma_2=\alpha_2}} = 0\ \Rightarrow\ \gamma_1 = \alpha_1 \quad (6)$$

$$\left.\frac{\partial \mathrm{Re}(\mathrm{CT}(\widehat{\Theta}))}{\partial \theta}\right|_{\substack{b=\tau, \\ \frac{w_0}{a}=w_c, \\ \gamma_2=\alpha_2}} = 0\ \Rightarrow\ \theta = \phi \pm 2k\pi, \quad k = 1, 2, 3, \ldots \quad (7)$$

The objective of the chirplet transform algorithm is to decompose the signal, into a linear expansion of chirplets and efficiently estimate the parameter vectors which define these chirplets (this is also known as adaptive chirplet transform ACT [30])

$$s(t) = \sum_{j=0}^{N-1} f_{\Theta_j}(t). \quad (8)$$

The parameter vector Θ_j can be estimated based on the chirplet transform of the signal. The time-of-arrival, center frequency, and amplitude of the dominant echo can be estimated by localizing the dominant echo in a time-frequency representation of the signal (i.e., chirplet transform), and then the remaining parameters can be successively estimated [27]. In an iterative manner, the residual signal is obtained by subtracting the estimated single dominant echo from the signal. The decomposition process is repeated until the energy of the residual signal reaches below a predefined reconstruction condition. The TF representation used for decomposition is computationally heavy due to the chirplet transform. In each iteration stage, the entire chirplet transform matrix is generated for the echo isolation process, which hinders the algorithm from real-time signal processing applications. This issue can be resolved by utilizing a fast implementation scheme of the algorithm [5], in which, instead of two-dimensional transform, a one-dimensional transform is used to iteratively estimate the time-of-arrival, center frequency, and amplitude of the dominant echo. Fig. 1 shows the flowchart of this fast chirplet transform (FCT) algorithm.

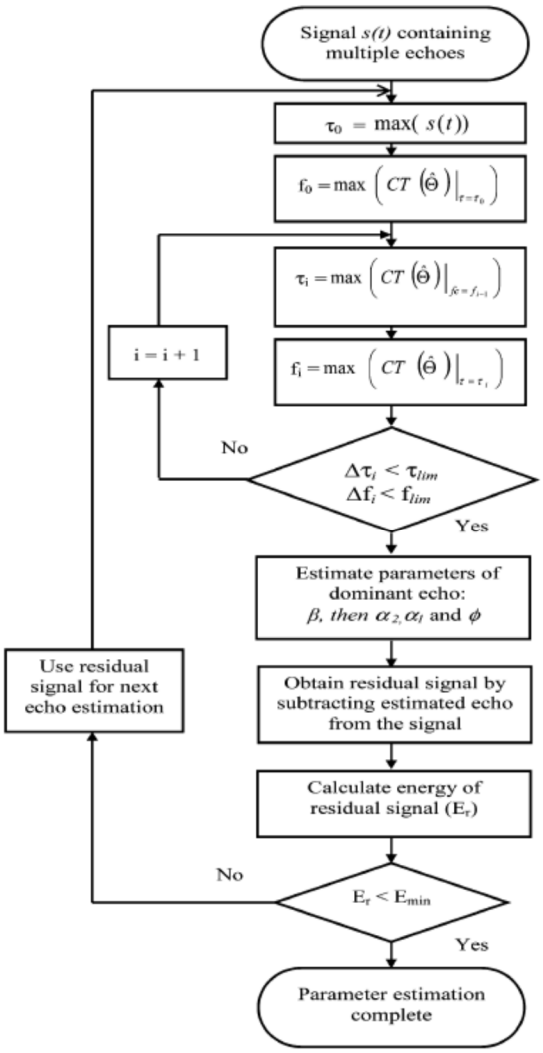

Fig. 1. Flowchart of the FCT algorithm [5]

A. Chirplet Decomposition of Experimental Data

The performance of the CSD algorithm is evaluated using both experimental data and simulation signals consisting of many interfering echoes. Fig. 2 shows the acquired signal testing of a steel block for flaw detection using a 5 MHz broadband transducer. The measured signal has poor SNR, and the flaw echo (marked target) is masked by the microstructure scattering and noise. The comparison between the measured signal and the reconstructed signal is shown in Fig. 2. This figure clearly demonstrates that the chirplet signal decomposition has been successful in estimating echoes while filtering out the noise. Moreover, the CSD algorithm is applied to a bat chirp signal emitted by the large brown bat [31], (see Fig. 3), which is digitized within a 2.2 ms duration with a 7 μs sampling period. It can be seen that from Fig. 3 the bat signal is a complex chirp with poor SNR and contains heavily overlapping, chirp components not only in the time domain but also in the frequency domain. Fig. 3(c) and 3(d) show the reconstructed signal and its CT using 15 individual chirplet echoes.

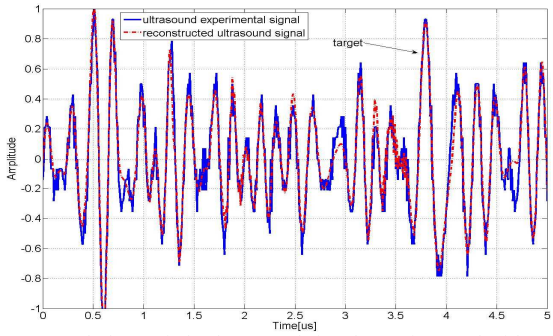

Fig. 2. Measured ultrasonic backscattered signal superimposed with a reconstructed signal [4]

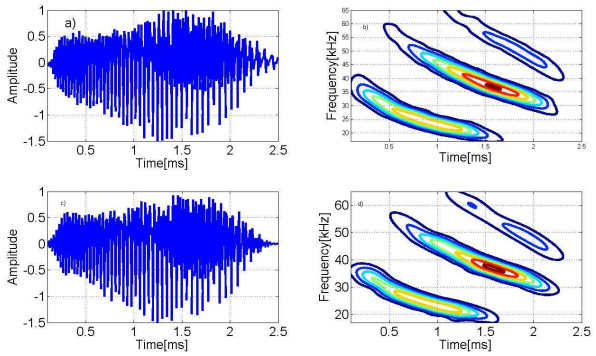

Fig. 3. (a) Experimental bat chirp signals. (b) CT of bat chirp signal in (a). (c) Reconstructed bat chirp signal. (d) CT of the reconstructed signal in (c).

B. CSD of Simulated Data with Poor SNR

The CSD-based successive parameter estimation can recover the exact value of the parameters of a noise-free Gaussian chirp echo, without requiring any initial guess for the parameters. Furthermore, the parameter estimation of a noise corrupted echo can be performed with high accuracy. To evaluate the performance of estimation, a Monte-Carlo simulation is performed to observe the means and variances of the estimated parameters of a single noisy echo. The chirp echo is simulated according to (1) with the parameter vector listed in the first row of Table 1. The noise level is adjusted to simulate echoes with SNR levels of 20, 15, 10, 5, and 2.5 dB. For each SNR level, the parameter estimation is performed 250 times on the simulated chirp echo with different realizations of noise. The average value and the variance of parameter estimators are listed in Table 1 along with the analytically computed CRLBs (Cramer Rao Lower Bounds) [26].

C. CSD Impact on Data Compression

Ultrasonic CSD modeling and echo estimation are powerful methods for both noise suppression (improving the SNR by an average of 40 dB) and data compression. In practice, a signal may contain several diagnostic echoes (for example, 20 echoes) while the captured signal may be represented by several thousand samples (e.g., 5000 acquired samples). Considering each echo contains 6 parameters: time-of-arrival, center

frequency, echo amplitude, chirp rate, phase, and bandwidth factor. Assuming each echo parameter and each data sample are represented by the same number of bits, the CSD representation of captured signal not only improves the SNR but also compresses the signal by 97%.

TABLE I. COMPARISON OF THE CRLBS WITH THE VARIANCES OF ESTIMATORS FOR DIFFERENT SNR

	α_1 [MHz]^2	α_2 [MHz]^2	τ [μs]	f_c [MHz]	ϕ [rad]	β
Actual Parameter	**25**	**15**	**1**	**5**	**1**	**1**
20.00 dB SNR						
MEAN	25.0266	15.0080	0.9999	4.9996	0.9959	1.0007
VARIANCE	4.4831e-1	5.6883e-1	4.5664e-6	3.4852e-4	4.5799e-3	1.5671e-4
CRLB	5.0000e-1	5.0000e-1	4.0000e-6	3.4449e-4	4.0978e-3	1.5000e-4
15.00 dB SNR						
MEAN	24.9987	15.0932	0.9997	4.9998	0.9906	0.9999
VARIANCE	1.5547	1.3617	1.2474e-5	1.2403e-3	1.3101e-2	4.8127e-4
CRLB	1.5811	1.5811	1.2649e-5	1.1000e-3	1.3000e-2	4.7434e-4
10.00 dB SNR						
MEAN	25.0242	14.8368	0.9997	4.9967	0.9911	1.0011
VARIANCE	4.0620	5.4588	3.5395e-5	3.4286e-3	3.4439e-2	1.4117e-3
CRLB	5.0000	5.0000	4.0000E-5	3.4000e-3	4.1000e-2	1.5000e-3
5.00 dB SNR						
MEAN	24.7932	15.2223	0.9997	4.9933	0.9905	1.0080
VARIANCE	14.4450	16.9490	1.3875e-4	1.1230e-2	1.4020e-1	3.8953e-3
CRLB	15.8114	15.8114	1.0000e-4	1.0900e-2	1.2960e-1	4.7000e-3
2.50 dB SNR						
MEAN	24.9589	15.0622	0.9981	4.9912	0.8623	1.0152
VARIANCE	33.4220	33.3590	2.1771e-4	2.0220e-2	6.2925e-1	9.6703e-3
CRLB	28.1171	28.1171	2.0000e-4	1.9400e-2	2.3040e-1	8.4000e-3

III. MULTILEVEL WPT-BASED COMPRESSION

For ultrasonic applications, a large portion of the signal energy is localized in the low-frequency region [32]. Consequently, the sub-bands with very low energy can be eliminated [33]. Multilevel WPT performs sub-band decomposition using lowpass and high pass filters [34]. The number of decomposition levels strictly depends on the nature of the signal, which governs the distribution of energy across the frequency bands. The objective is to determine the most suitable wavelet kernel for a given signal in terms of maximum energy compaction within a sub-band. This depends on the extent of similarity of the wavelet kernels with the ultrasonic RF signals. The different families of wavelets examined in this study are Daubechies (D4, D6, D8, and D10), Symlet (5,6,7, and 8); Coiflet (2,3,4, and 5), and Haar. Daubechies-10, Symlet-6/8, and Coiflet-5 consistently performed better than the other kernels within their family.

Fig. 4 demonstrates the efficiency of wavelet packet decomposition of an ultrasonic A-scan with 2048 samples consisting of many reflected and interfering echoes. This figure indicates that the relevant information within the signal is localized in the low-frequency sub-bands. Furthermore, {H, LH, and LLHL} sub-bands which constitute 79% of the signal samples have almost zero energy and can be discarded, indicating 79% compression.

A. Ultrasonic Data Acquisition and 3D Data Compression

Industrial NDE and medical imaging applications require volumetric data processing. This information is collected by the process of 3D scanning and massive RF signal data acquisition, which needs to be carefully compressed. In volumetric ultrasonic data compression, data sets (slices) are organized into a 3D block (128*128*2048 samples) as shown in Fig. 5 and subsequently, this block of data is compressed to remove the inter-slice data redundancy in x, y, and z directions as shown in Fig 5b.

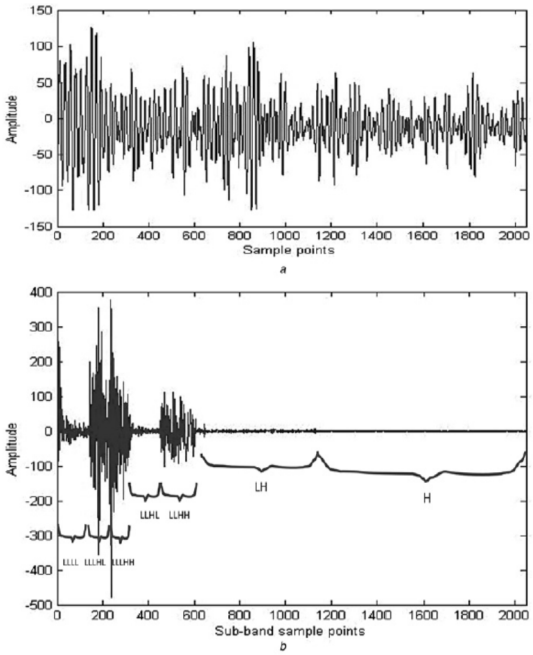

Fig. 4. Ultrasonic A-scan with 2048 samples consisting of many reflected and interfering echoes and the decomposed sub-bands

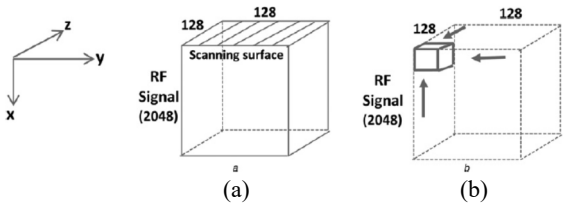

(a) (b)

Fig. 5. Data sets (slices) are organized into a 3D block; (a) 3D ultrasonic data block, (b) 3D compressed data block

Fig. 6a shows the block diagram of the ultrasonic scanning and testing setup. In this study, a 5 MHz, 0.375-inch diameter ultrasonic broadband transducer (A3062) along with a pulser/receiver model 5052 PR is used to acquire a 3D block of data from a steel block specimen with microstructural defects. A 2 x 2 inch surface of the steel block specimen is used to generate this experimental data, which consists of a volumetric image of 128×128×2048 samples (33 MB when each sample is represented using 1 byte). The acquired volumetric data consists of interfering echoes [35] which represent the microstructural scattering of materials.

Measurement points are very close to each other (0.44 mm) to ensure no information is missed out within the specimen under test. Since the neighboring measurement points will have plenty of similarities, this can be utilized for better compression of the data. In this study, the original 3D block of data as shown in Fig. 5a is compressed using successive 1D compressions in the x, y, and z directions [34].

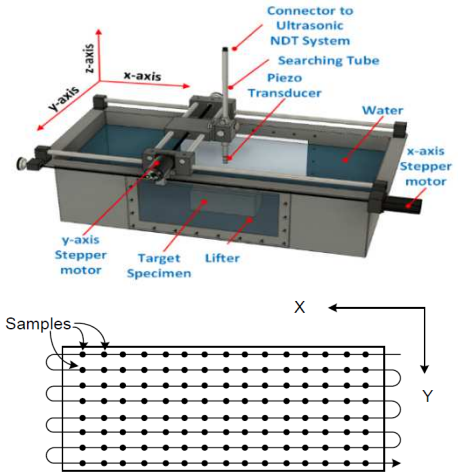

Fig. 6. Ultrasonic volumetric scanning setup; (a) Block diagram of an ultrasound scanning system, (b) Scanning pattern of the transducer

In order to accomplish maximum compression in the x-direction, a 4-level wavelet packet decomposition [36], [37] structure as shown in Fig. 7 is designed to isolate the high energy frequency sub-bands. Since the 3D compression ratio is not heavily influenced by the compression in y and z directions, a simple Haar wavelet is used for decomposition in y and z directions. Our experimentations indicate 80% compression in x-direction. An additional 75% compression is achieved in the y-direction and a further 75% compression in the z-direction. As a result, the overall 3D compression becomes 98.7% [34]. This indicates that only 1.3% of the total 3D volumetric data needs to be retained and transferred to remote locations, from which the whole 3D block of data can be reconstructed back with a very high degree of similarity. Ultrasonic 3D RF data compression algorithms are analyzed based on the degree of compression of RF data as a function of data integrity. Fig. 8 shows the original and reconstructed A-scans for 80%, 95%, and 98.7% compression respectively, wherein, for 80% compression, the reconstruction quality is extremely high, and for 95% and 98.7%, the reconstructed signal follows the original signal with only minor variations, indicating the efficiency of the compression without losing the relevant information.

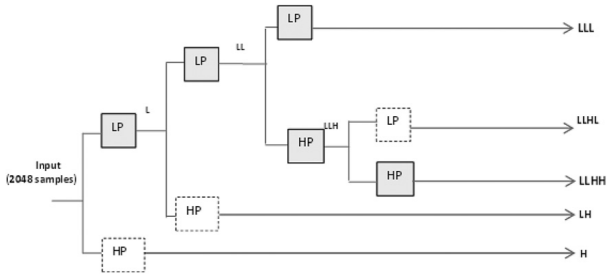

Fig. 7. Wavelet packet decomposition in the x-direction (since only LLL and LLHH are retained, the filters in the dashed line are not required in the implementation)

IV. WPT Convolutional Auto Encoder (WPTCAE)

Even though WPT compression provides a very high level of compression, the efficiency of compression highly depends on the similarity of the wavelet kernel used and the application signal. To further enhance the compression performance for a broad range of applications, a WPTCAE compression system is proposed which uses training models to choose the most optimal wavelet kernel and the decomposition tree structure. Fig. 9 illustrates the design flow of the WPTCAE compression system [38]. From the acquired ultrasonic data (Fig. 9A), a few random samples are chosen to find an optimal WPT compression and reconstruction tree structure for a given ultrasonic dataset (Fig 9B). By using the initial coefficients from the above step, the WPT encoder and decoder are trained

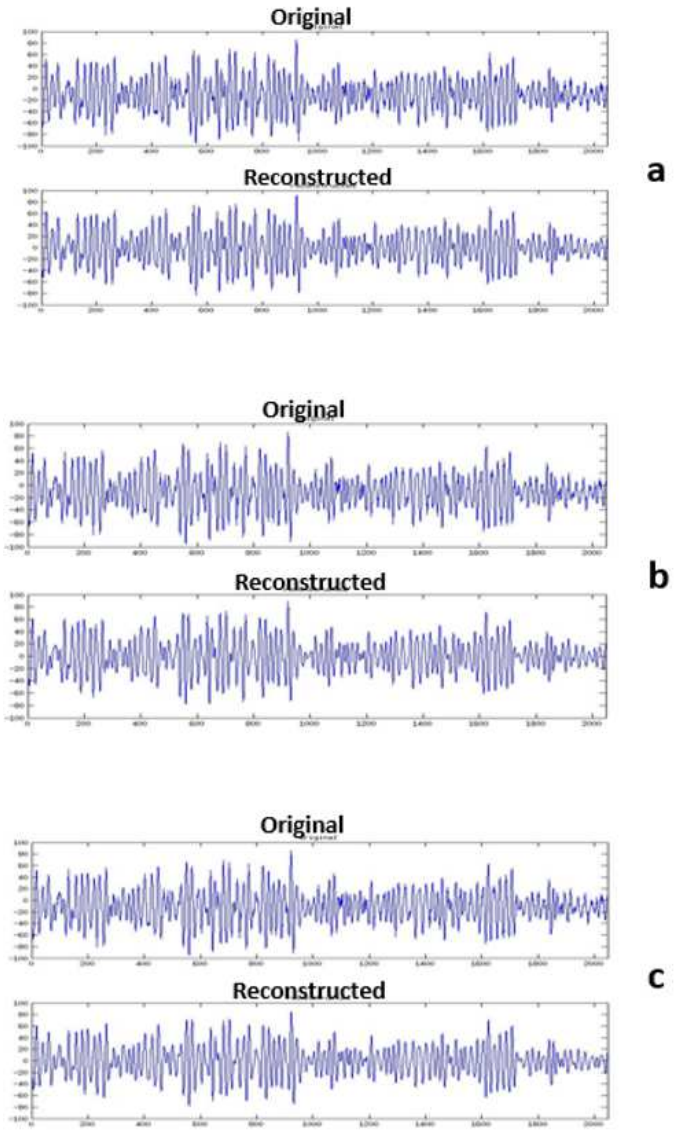

Fig. 8. WPT Performance for 3D RF Ultrasonic Data Compression; (a) Original & Reconstructed A-scan for 80% compression, (b) Original & Reconstructed A-scan for 95% compression, (c) Original & Reconstructed A-scan for 98.7% compression

using the backpropagation algorithm (Fig. 9C). This trained WPTCAE model is used for efficient data compression and reconstruction (Fig. 9D). In this study, the WPTCAE compression model is benchmarked by using two types of ultrasonic image datasets: (i) Ultrasonic NDT data [39], and (ii) Open Access Series of Breast Ultrasonic Data (OASBUD) [40].

Fig. 10 shows the plot and the power spectral density (PSD) of a randomly selected ultrasonic A-Scan from the NDT dataset, with 2048 data points. The measured A-Scan, which represents the microstructure (grains) scattering within the steel block [41], [42], consists of multiple interfering echoes with random amplitudes and arrival times.

Fig. 11 shows a randomly selected A-Scan and its PSD from the OASBUD dataset, which represents ultrasonic backscattered echoes from breast lesions of patients [40], acquired with a sampling frequency of 40-MHz.

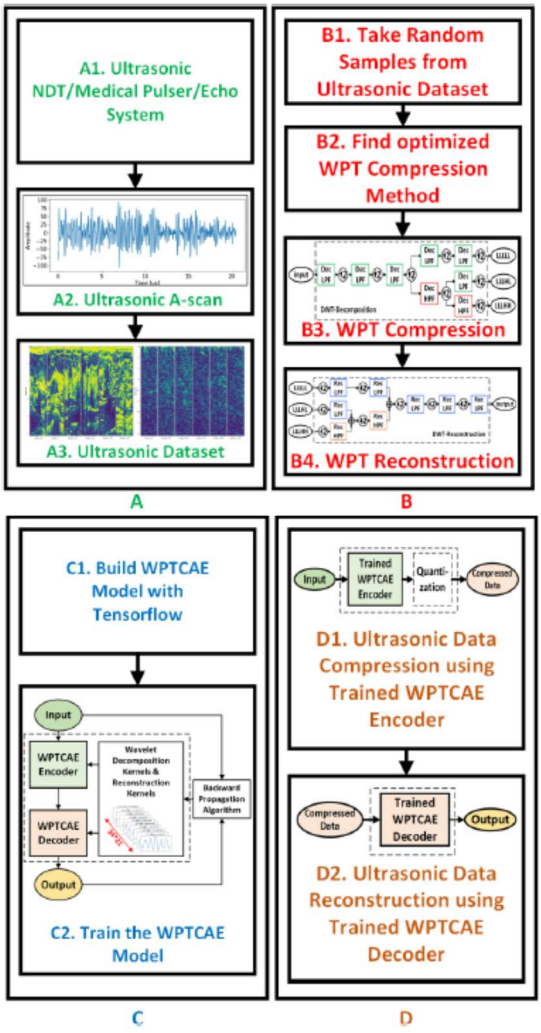

Fig. 9. Design flow of WPT optimized by a CAE for ultrasonic data compression. (A) Ultrasonic data acquisition. (B) WPT compression optimization. (C) WPTCAE model. (D) WPTCAE compression and reconstruction.

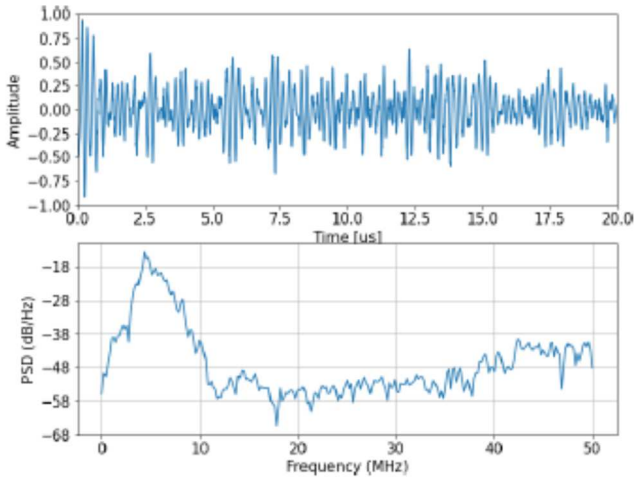

Fig. 10. Ultrasonic NDT backscattered A-scan from a steel block and the PSD. The dataset is acquired using an immersive ultrasonic transducer centered at 5 MHz with a sampling frequency of 100 MHz.

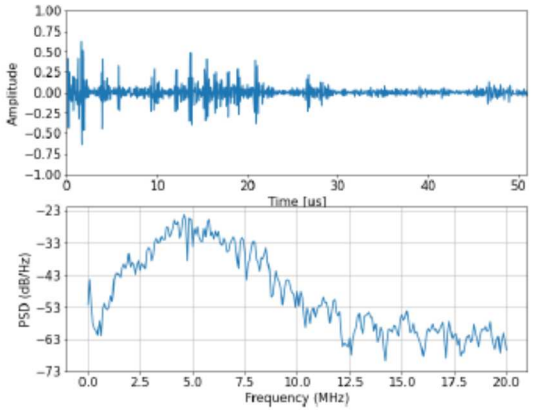

Fig. 11. Ultrasonic medical backscattered A-scan and the PSD. The dataset is acquired using an ultrasonic linear array transducer centered at 5 MHz with a sampling frequency of 40 MHz.

A. Training Data Compression Models using Ultrasonic Experimental Data

This study proposes unsupervised learning models for the following data compression algorithms: AE, CAE, WPTCAE, and a WPTCAE/AE hybrid model [38]. For improved compression accuracy, a hybrid model referred to as WPTCAE/AE is also designed that combines the AE and WPTCAE models. The AE model, after learning a linear transformation, projects the data onto another space (i.e., bottleneck) with fewer dimensions. This is equivalent to a principal component analysis (PCA) model. Training an AE model for compression minimizes the *mean square error* between the input and the output using the backpropagation algorithm [43].

The CAE model (shown in Fig. 12) generally includes one or more convolution layers before the AE encoder, (where the signal is downsampled by 2) and after the AE decoder (where the signal is upsampled by 2).

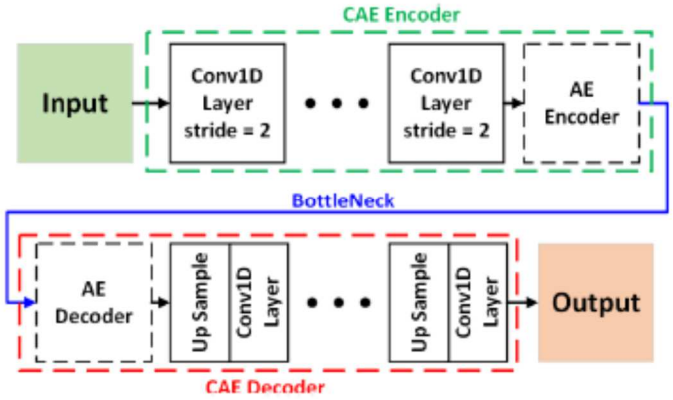

Fig. 12. General block diagram of the CAE

In this study, a Python script is developed [38] to iterate through 106 discrete wavelet filters available in PyWavelets library [44], to find the optimal kernel for the ultrasonic datasets. This algorithm is applied to both ultrasonic NDT [39] and OASBUD datasets [40]. Fig. 13 shows the decomposition and reconstruction filter kernels of "coif17" from the Coiflet wavelet family (optimal for NDT) and "db36" from the Daubechies wavelet family (optimal for OASBUD). Fig. 14 and Fig. 15 illustrate the trained encoder and decoder for the ultrasonic NDT dataset and OASBUD dataset respectively [38]. To minimize the amount of lost information during the WPT compression, a WPTCAE/AE hybrid model is proposed, wherein the same input is applied to both WPTCAE and CE models, and the sum of the predictions from both is used as the output. This helps to further improve the reconstruction quality.

B. Compression Results and Performance Analysis of WPT, WPTCAE, and WPTCAE/AE

For the compression performance analysis, the input data, compressed data, reconstructed data, and model weights are considered to be 32-bit floating-point numbers. The search for the optimal data compression models is achieved through 150 epochs of training [38]. Fig. 16 shows the time-domain comparison of randomly selected A-Scans and B-scans from the ultrasonic NDT and OASBUD datasets and their reconstructions. Compared with the conventional WPT algorithm, the WPTCAE compression model displays exceptional compression accuracy and reconstructed signal accuracy, along with SNR improvement for both of the datasets.

Another important characteristic of compression algorithms is the data bit precision. The ultrasonic NDT and OASBUD 32-bit floating-point datasets are scaled and quantized into 8-bit precision numbers. The sub-bands of the compressed output are quantized into 8 bits or fewer in order to increase the compression ratio. Fig. 17 indicates that the quantization helps to increase the compression ratio substantially, while the reduction in compression accuracy is insignificant.

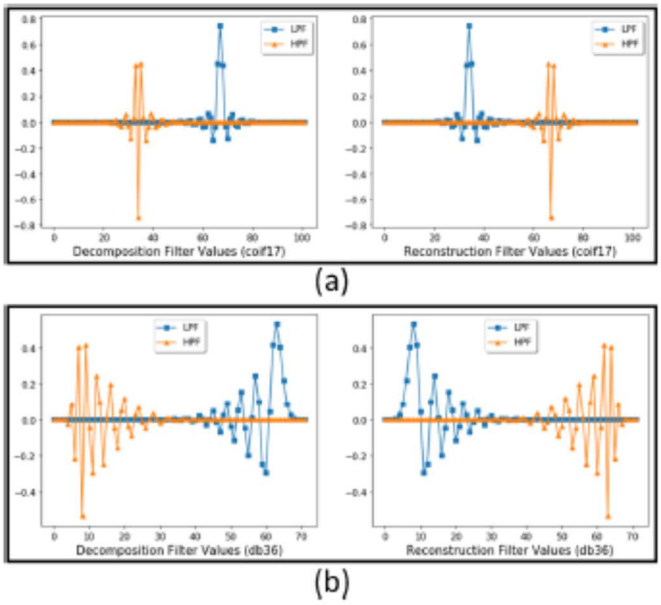

Fig. 13. WPT filter decomposition and reconstruction analysis and synthesis filter kernels. (a) "coif17" from the Coiflet wavelet family. (b) "db36" from the Daubechies wavelet family.

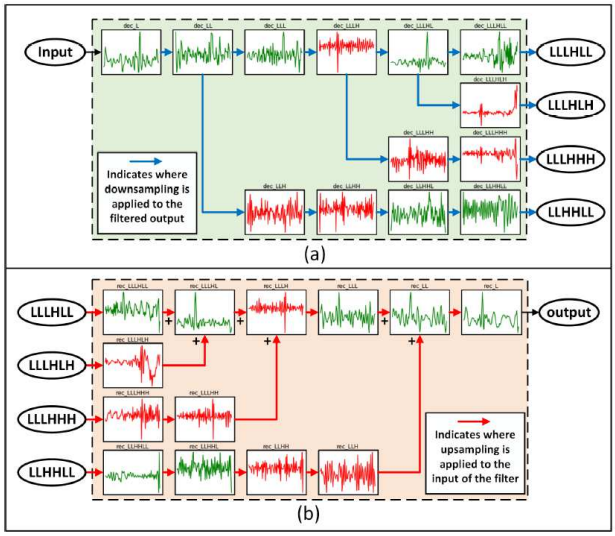

Fig. 14. Trained encoder (a) and decoder (b) for the ultrasonic NDT dataset.

V. CONCLUSION

The WPTCAE data compression algorithm, the unsupervised learning data compression methods such as AE, and chirplet modeling of ultrasonic signals for high-fidelity data analysis and compression are applied to ultrasonic RF datasets acquired in NDT and medical imaging applications. A successive parameter estimation algorithm based on CT, and an automatic echo windowing method have been developed to estimate the time of arrival, the center frequency, the phase, the bandwidth, the chirp rate, and the amplitude of chirp echoes. Monte-Carlo simulation results demonstrate that the successive parameter estimation is unbiased and exhibit minimum variance, i.e., the

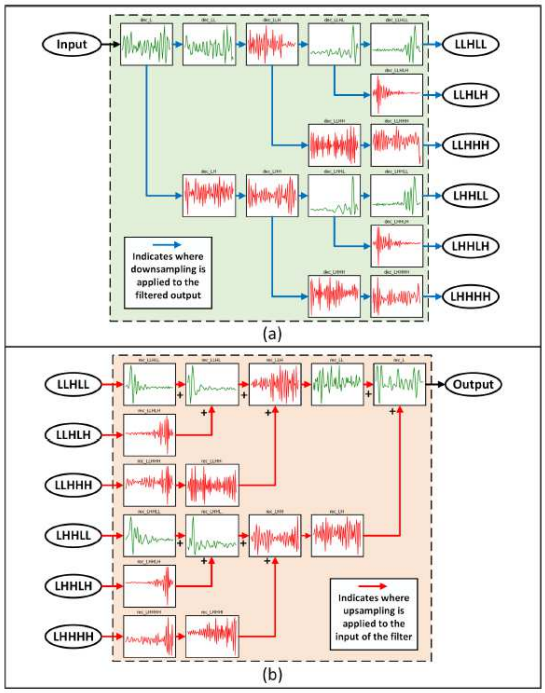

Fig. 15. Trained encoder (a) and decoder (b) for the ultrasonic OASBUD dataset.

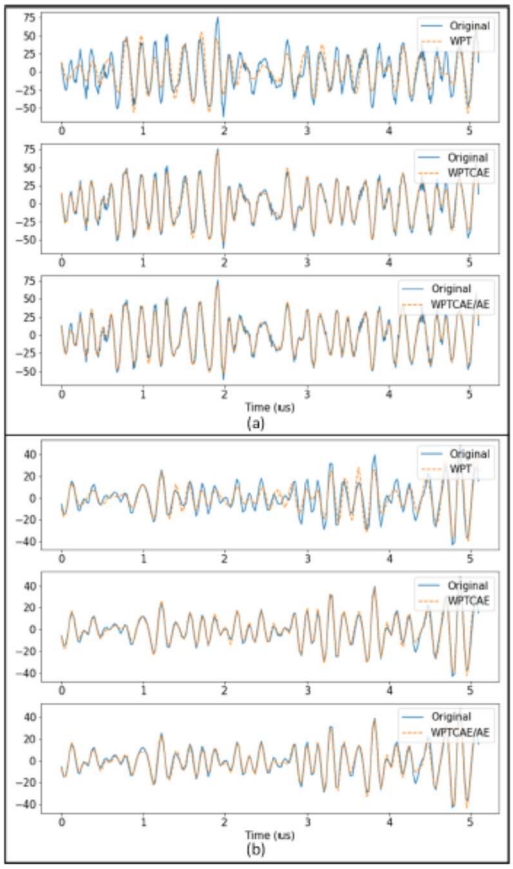

Fig. 16. Comparison of the original A-scans and the reconstructed signals using the WPT, WPTCAE, and WPTCAE/AE compression models; (a) NDT dataset. (b) OASBUD dataset.

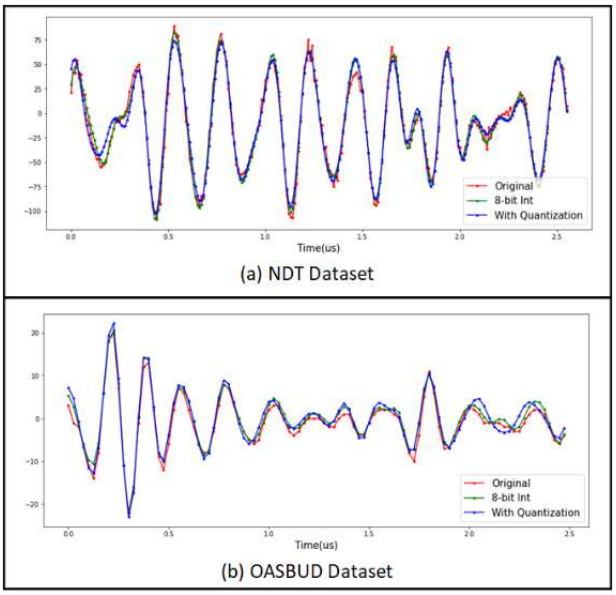

Fig. 17. Comparison between the original A-scans and the reconstructed signals of the WPTCAE compression models when quantization is introduced into the algorithm; (a) NDT dataset, with the sub-bands quantized into 5, 4, 6, and 7 bits, (b) OASBUD dataset, with sub-bands quantized into 4, 4, 7, 4, 4, and 7 bits.

variances in the parameter estimators attain the CRLB. The experimental results for WPT compression methods clearly show that the WPTCAE data compression model provides improved compression ratios while maintaining high signal fidelity with a compression accuracy of 98% by using only 6% of the original data. Furthermore, by using unsupervised learning for high compression performance, an average compression ratio of 95.75% is achieved. This study also demonstrates that 33 MB of experimental ultrasonic 3D data can be compressed into 0.42 MB, providing a very high level of compression, almost close to 99%.

REFERENCES

[1] Scabia, M., Biagi, E., Masotti, L.: 'Hardware and software platform for real-time processing and visualization of Echographic radio frequency signals', IEEE Trans. Ultrason. Ferroelectr. Freq. Control, 2002, 49, (10), pp. 1444–1452.

[2] Saniie, J., Wang, T., Jin, X.: 'Performance evaluation of frequency diverse bayesian ultrasonic flaw detection', J. Acoust. Soc. Am., 1992, 91, (4), Pt. 1, pp. 2034–2041.

[3] Wang, T., Saniie, J., Jin, X.: 'Analysis of low-order autoregressive models for ultrasonic grain signal characterization', IEEE Trans. Ultrason. Ferroelectr. Freq. Control, 1991, 38, (2), pp. 116–124.

[4] Lu, Y., G. Cardoso, R. Demirli, and J. Saniie, "Chirplet transform for ultrasonic signal analysis and NDE applications," in *Proc. IEEE Ultrason. Symp.*, Sep. 2005, pp. 536–539.

[5] Lu, Y., E. Oruklu and Jafar Saniie, Fast chirplet transform with FPGA-based implementation, *IEEE Signal Processing Letters*, 2008, pp 577-580.

[6] J. Li and H. Ling, "Application of adaptive chirplet representation for ISAR feature extraction from targets with rotating parts," *IEE Proc. Radar, Sonar, Navigation*, vol. 150, pp. 284–291, Aug. 2003.
[7] W. Fan, H. Zou, Y. Sun, Z. Li, and R. Shi, "Decomposition of seismic signal via chirplet transform," in *Proc. IEEE 6th Int. Conf. Signal Processing*, Aug. 2002, pp. 1778–1782.
[8] N. Ma and D. Vray, "Bottom backscattering coefficient estimation from wideband chirp sonar echoes by chirp adapted time frequency representation," in *Proc. IEEE Int. Conf., Acoust., Speech Signal Processing*, May 1998, pp. 12–15.
[9] G. Lopez-Risueno, J. Grajal, and O. A. Yeste-Ojeda, "CFAR detection of chirplets in coloured Gaussian noise," in *Proc. IEEE Conf., Acoust., Speech Signal Processing*, Apr. 2003, pp. 741–744.
[10] S. Krishnamachari and W. J. Williams, "Adaptive kernel design in the generalized marginal domain for time-frequency analysis," in *Proc. IEEE Int. Conf., Acoust., Speech, Signal Processing*, Apr. 1994, pp. 341–344.
[11] S. Mann and S. Haykin, "The chirplet transform: Physical considerations," *IEEE Trans. Signal Processing*, vol. 43, no. 11, Nov. 1995, pp. 2745–2761.
[12] S. Mann and S. Haykin, "Time-frequency perspectives: The chirplet transform," in *Proc. IEEE Int. Conf., Acoust., Speech Signal Processing*, Mar. 1992, pp. 417–420.
[13] S. Qian, D. Chen, and Q. Yin, "Adaptive chirplet based signal approximation," in *Proc. IEEE Int. Conf., Acoust., Speech, Signal Processing*, May 1998, pp. 1781–1784.
[14] A. Feng, X. Wu, and Q. Yin, "Fast algorithm of adaptive chirplet-based real signal decomposition," in *Proc. IEEE Int. Symp. Circuits Syst.*, Mar. 2001, pp. 6–9.
[15] X. Xia, "Discrete chirp-Fourier transform and its application to chirp rate estimation," *IEEE Trans. Signal Processing*, vol. 48,pp. 3122–3133, Nov. 2000.
[16] P. M. Djuric and S. M. Kay, "Parameter estimation of chirp signals," *IEEE Trans. Acoust. Speech Signal Processing*, vol. 38, Dec. 1990, pp. 2118–2126.
[17] R. Demirli and J. Saniie, "Model-based estimation of ultrasonic echoes. Part II: Nondestructive evaluation applications," *IEEE Trans. Ultrason., Ferroelect., Freq. Contr.*, vol. 48, May 2001, pp. 803–811.
[18] R. Demirli and J. Saniie, "Model based time-frequency estimation of ultrasonic echoes for NDE applications," in *Proc. IEEE Ultrason. Symp.*, Oct. 2000, pp. 785–788.
[19] S. M. Kay, *Fundamentals of Statistical Signal Processing: Estimation Theory*. Englewood Cliffs, NJ: Prentice-Hall, 1998.
[20] Daubechies, I.: 'Ten Lectures on Wavelets'. CBMS-NSF Regional Conference Series in Applied Math, SIAM, Philadelphia, 1992, vol. 61
[21] Vetterli, M., Herley, C.: 'Wavelets and filter banks: theory and design', IEEE Trans. Signal Process., 1992, 40, (9), pp. 2207–2232.
[22] F. N. Khan and A. P. T. Lau, "Robust and efficient data transmission over noisy communication channels using stacked and denoising autoencoders," *China Commun.*, vol. 16, no. 8, Aug. 2019, pp. 72–82.
[23] Y. H. Lai, F. Chen, S.-S. Wang, X. Lu, Y. Tsao, and C.-H. Lee, "A deep denoising autoencoder approach to improving the intelligibility of vocoded speech in cochlear implant simulation," *IEEE Trans. Biomed. Eng.*, vol. 64, no. 7, Sep. 2017, pp. 1568–1578.
[24] D. Del Testa and M. Rossi, "Lightweight lossy compression of biometric patterns via denoising autoencoders," *IEEE Signal Process. Lett.*, vol. 22, no. 12, Dec. 2015, pp. 2304–2308.
[25] Z. Cheng, H. Sun, M. Takeuchi, and J. Katto, "Energy compaction based image compression using convolutional autoencoder," *IEEE Trans. Multimedia*, vol. 22, no. 4, Apr. 2020, pp. 860–873.
[26] Y. Lu, R. Demirli, G. Cardoso, and J. Saniie, "A successive parameter estimation algorithm for chirplet signal decomposition," *IEEE Trans. Ultrason., Ferroelect., Freq. Control*, vol. 53, no. 11, Nov. 2006, pp. 2121–2131.
[27] S. Mann and S. Haykin, "The chirplet transform: Physical consideration," *IEEE Trans. Signal Process.*, vol. 43, no. 11, Nov. 1995, pp. 2745–2761.
[28] S. Mann and S. Haykin, "The chirplet transform: A generalization of Gabor's logon transform," in *Proc. Vision Interface'91*, Jun. 1991, pp. 205–212.
[29] G. Lopez-Risueno, J. Grajal, and O. A. Yeste-Ojeda, "CFAR detection of chirplets in coloured Gaussian noise," in *Proc. IEEE Conf., Acoust., Speech Signal Processing*, Apr. 2003, pp. 741–744.
[30] S. Mann and S. Haykin, "The adaptive chirplet: An adaptive wavelet like transform," in *Proc. SPIE, 36th Annu. Int. Symp. Optical and Optoelectronic Applied Science and Engineering*, Jul. 1991.
[31] C. Condon, K. White, and A. Feng, The bat data, Beckman Institute of the University of Illinois, Urbana, IL, http://wwwdsp.rice.edu/software/bat.shtml
[32] Vetterli, M., Herley, C.: 'Wavelets and filter banks: theory and design', IEEE Trans. Signal Process., 1992, 40, (9), pp. 2207–2232.
[33] Oruklu, E., Jayakumar, N., Saniie, J.: 'Ultrasonic signal compression using wavelet packet decomposition and adaptive Thresholding'. IEEE Ultrasonics Symp., 2008, pp. 171–175
[34] Govindan, P., Saniie, J.: 'Processing algorithms for three-dimensional data compression of ultrasonic radio frequency signals', IET Signal Process., 2015, 9, (3), pp. 267–276.
[35] Saniie, J.: 'Ultrasonic signal processing: system identification and parameter estimation of reverberant and inhomogeneous targets'. PhD thesis, Department of Electrical Engineering, Purdue University, West Lafayette, IN, 1981
[36] Djawad, Y.A., Kiely, J., Nibouche, M., Wraith, P., Luxton, R.: 'Robust feature extraction from impedimetric signals using wavelet packet decomposition with application to cytotoxicity testing', IET Sci. Meas. Technol., 2012, 6, (6), pp. 456–463.
[37] Govindan, P., Saniie, J.: 'Performance evaluation of 3D compression for ultrasonic nondestructive testing applications'. IEEE Int. Ultrasonics Symp. (IUS), July 2013, pp. 437–440.
[38] B. Wang and J. Saniie, "Massive ultrasonic data compression using wavelet packet transformation optimized by convolutional autoencoders," IEEE Transaction on Neural Networks and Learning Systems, Sep. 2021, pp. 1–11.
[39] P. Govindan, B. Wang, P. Ravi, and J. Saniie, "Hardware and software architectures for computationally efficient three-dimensional ultrasonic data compression," *IET Circuits Devices Syst.*, vol. 10, no. 1, Jan. 2016, pp. 54–61.
[40] H. Piotrzkowska-Wróblewska, K. Dobruch-Sobczak, M. Byra, and A. Nowicki, "Open access database of raw ultrasonic signals acquired from malignant and benign breast lesions," *Med. Phys.*, vol. 44, no. 11, pp. 6105–6109, Nov. 2017, doi: 10.1002/mp.12538.
[41] J. Saniie, T. Wang, and N. M. Bilgutay, "Analysis of homomorphic processing for ultrasonic grain signal characterization," *IEEE Trans. Ultrason., Ferroelectr., Freq. Control*, vol. 36, no. 3, May 1989, pp. 365–375.
[42] J. Saniie and N. M. Bilgutay, "Quantitative grain size evaluation using ultrasonic backscattered echoes," *J. Acoust. Soc. Amer.*, vol. 80, no. 6, pp. 1816–1824, Dec. 1986, doi: 10.1121/1.394296.
[43] H. J. Kelley, "Gradient theory of optimal flight paths," *ARS J.*, vol. 30, no. 10, 1960, pp. 947–954.
[44] G. R. Lee, R. Gommers, F. Waselewski, and K. Wohlfahrt, "Pywavelets: A Python package for wavelet analysis," *J. Open Source Softw.*, vol. 4, no. 36, p. 1237, 2019, doi: 10.21105/joss.01237.